Similarities and differences in the transcriptional control of expression of the mouse TSLP gene in skin epidermis and intestinal epithelium

Krishna Priya Ganti[a,b,c], Atish Mukherji[a,b,c,1], Milan Surjit[a,b,c,d,1], Mei Li[a,b], and Pierre Chambon[a,b,c,2]

[a]Institut de Génétique et de Biologie Moléculaire et Cellulaire (CNRS UMR7104, INSERM U964), Illkirch 67404, France; [b]University of Strasbourg Institute for Advanced Study, F-67083 Strasbourg, France; [c]Collège de France, 75005 Paris, France; and [d]Translational Health Science and Technology Institute, National Capital Region Biotech Science Cluster, Faridabad-121001, India

Contributed by Pierre Chambon, December 20, 2016 (sent for review November 18, 2016; reviewed by Christophe Benoist, Didier Picard, and Filippo M. Rijli)

We previously reported that selective ablation of the nuclear receptors retinoid X receptor (RXR)-α and RXR-β in mouse epidermal keratinocytes (RXR-αβ$^{ep-/-}$) or a topical application of active vitamin D3 (VD3) and/or all-trans retinoic acid (RA) on wild-type mouse skin induces a human atopic dermatitis-like phenotype that is triggered by an increased expression of the thymic stromal lymphopoietin (TSLP) proinflammatory cytokine. We demonstrate here that in epidermal keratinocytes, unliganded heterodimers of vitamin D receptor (VDR)/RXR-α and retinoic acid receptor-γ (RAR-γ)/RXR-β are bound as repressing complexes to their cognate DNA-binding sequence(s) (DBS) in the TSLP promoter regulatory region. Treatments with either an agonistic VD3 analog or RA dissociate the repressing complexes and recruit coactivator complexes and RNA polymerase II, thereby inducing transcription. Furthermore, we identified several functional NF-κB, activator protein 1 (AP1), STAT, and Smad DBS in the TSLP promoter region. Interestingly, many of these transcription factors and DBS present in the TSLP promoter region are differentially used in intestinal epithelial cell(s) (IEC). Collectively, our study reveals that, in vivo within their heterodimers, the RXR and RAR isotypes are not functionally redundant, and it also unveils the combinatorial mechanisms involved in the tissue-selective regulation of TSLP transcription in epidermal keratinocytes and IEC.

TSLP transcription | nuclear receptors | skin | intestine | NF-κB

We reported that keratinocyte-selective ablation of retinoid X receptor (RXR)-α and RXR-β in epidermal keratinocytes of the mouse (RXR-αβ$^{ep-/-}$ mutants) results in a skin and systemic syndrome that mimics human atopic dermatitis (AD) and is preceded, in epidermal keratinocytes, by enhanced expression of the thymic stromal lymphopoietin (TSLP) cytokine (1). Moreover, several lines of evidence have revealed that TSLP expression is both necessary and sufficient to induce an atopic inflammation in the mouse (1–4). TSLP, which is also expressed in human AD skin lesions (5, 6), has been considered to be the master regulator of allergic inflammation (7).

Interestingly, the TSLP promoter region was found to contain several putative nuclear receptor (NR) DNA-binding sequence(s) (DBS) (2). Topical treatment with active vitamin D3 [1α, 25(OH)2 (VD3)] or its low-calcemic analog calcipotriol (also named MC903; hereafter, MC), all-trans retinoic acid (RA), and the retinoic acid receptor-γ (RAR-γ)–selective retinoid BMS961, which are agonistic ligands for vitamin D receptor (VDR), all three RARs, and RAR-γ, respectively, could induce TSLP expression in mouse keratinocytes on their own or synergistically (2). However, MC was more efficient than BMS961 at inducing TSLP expression in these cells, and long-term treatment with MC resulted in an AD-like syndrome similar to the syndrome observed in RXR-αβ$^{ep-/-}$ mice. To reveal how both the keratinocyte-selective ablation of RXR-α and RXR-β (RXR-γ is not expressed in keratinocytes) or MC and/or BMS961 treatments could induce TSLP expression, we posited that because there is no RA and very little, if any, VD3 in keratinocytes (2) under in vivo homeostatic conditions, the activity of the TSLP promoter could be repressed by corepressor-bound unliganded RXR-α (or RXR-β)/VDR and RXR-α (or RXR-β)/RAR-γ heterodimers bound to VDR and RAR response elements (VDRE and RARE, respectively). Thus, RXR-α and RXR-β ablations, which release both heterodimers from their DBS, might abolish repression and allow other promoter-bound transcription factors (TFs) to stimulate TSLP transcription. Moreover, MC application would generate RXR/VDR-coactivator complexes, the transcriptional activity of which would be sufficient to overcome the repression exerted by RXR/RAR-γ corepressor complexes, thereby enhancing the basal promoter activity, whereas RXR/RAR-γ coactivator complexes formed upon application of BMS961, would be less efficient at relieving the repression exerted by RXR/VDR-corepressor complex (figure 5 of ref. 2).

We investigated here the validity of such a mechanism through which RXR/VDR and RXR/RAR-γ heterodimers regulate TSLP expression. We also characterized DBS for additional TFs, which can function independent of RAR-γ and VDR. Furthermore, because TSLP is also expressed in intestinal epithelial cell(s) (IEC), we compared the binding pattern of TFs associated with the TSLP promoter region in epidermis and IEC and revealed striking differences between these tissues. Taken together, our studies unveil the complex organization of the TSLP promoter, and demonstrate how TSLP expression is controlled at the transcriptional level in mouse epidermis and IEC.

Significance

Thymic stromal lymphopoietin (TSLP) is a critical immunoregulatory cytokine that plays important physiological functions in epithelial cells in skin and intestinal barriers. However, the molecular mechanisms controlling TSLP expression in vivo are still poorly understood. Using tissue-selective mutagenesis in mice, we have identified the involvement of multiple transcriptional factors, including several nuclear receptors and their cognate agonistic ligands, in the transcriptional regulation of TSLP in epidermal keratinocytes and intestinal epithelial cells. Importantly, this investigation also demonstrates that the retinoid X receptor (RXR) and retinoic acid receptor (RAR) isotypes are not functionally redundant in vivo. Taking our data together, the present study unveils the topological map and the combinatorial mechanisms involved in tissue-specific transcriptional regulation of TSLP expression in epidermal keratinocytes and intestinal epithelial cells.

Author contributions: K.P.G., A.M., M.S., and P.C. designed research; K.P.G., A.M., and M.S. performed research; M.L. contributed new reagents/analytic tools; K.P.G., A.M., M.S., and P.C. analyzed data; and A.M. and P.C. wrote the paper.

Reviewers: C.B., Harvard Medical School; D.P., University of Geneva; and F.M.R., Friedrich Miescher Institute for Biomedical Research.

The authors declare no conflict of interest.

[1]A.M. and M.S. contributed equally to this work.

[2]To whom correspondence should be addressed. Email: chambon@igbmc.fr.

This article contains supporting information online at www.pnas.org/lookup/suppl/doi:10.1073/pnas.1620697114/-/DCSupplemental.

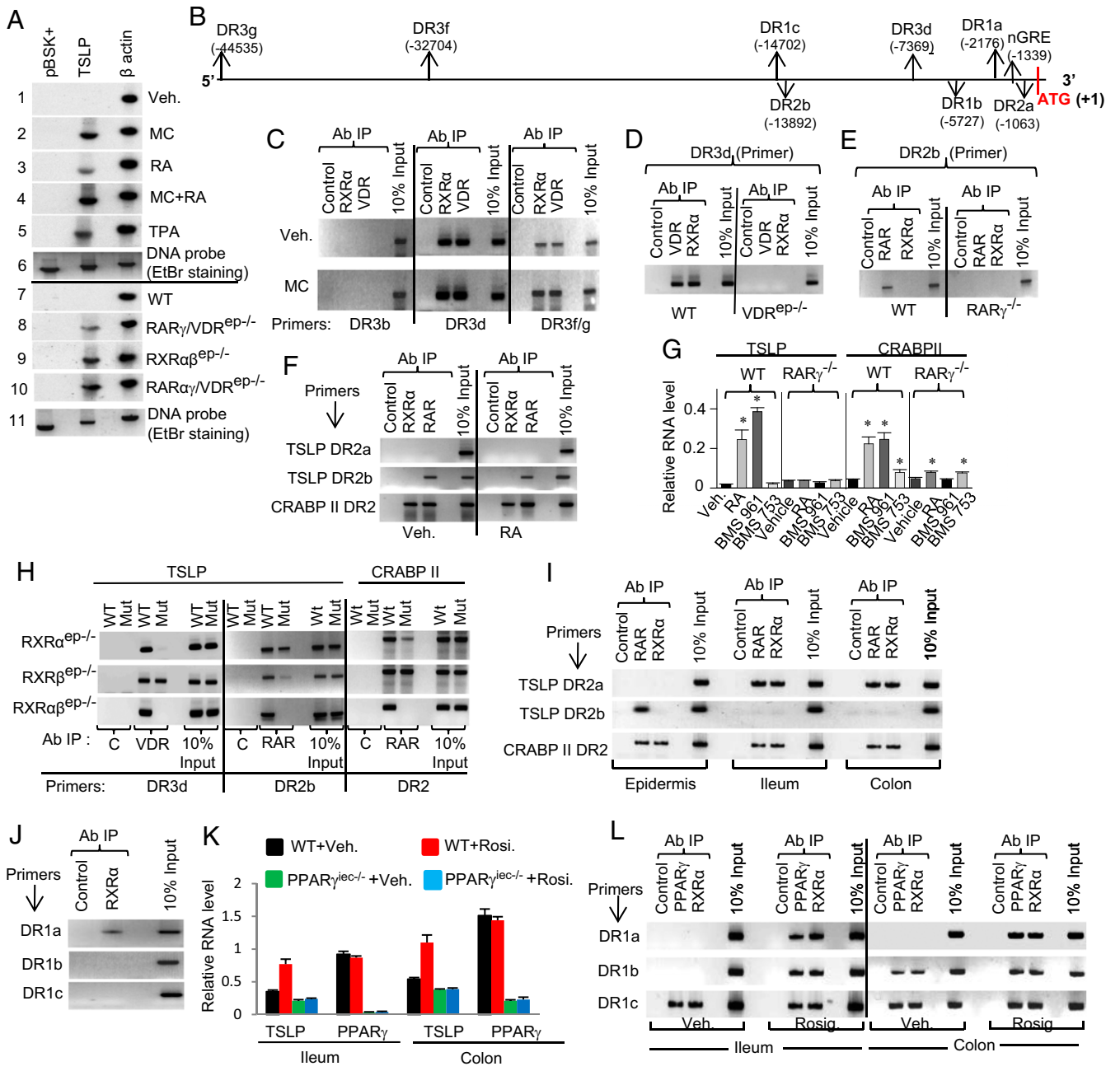

Fig. 1. Multiple NRs regulate TSLP expression in the mouse epidermal keratinocytes and in IEC. (*A*) Nuclear run-on assay using epidermis from WT mice treated as indicated (panels 1–5 and panel 7) or from different keratinocyte-selective mutants (panels 8–10). Autoradiograms of labeled transcripts hybridized with TSLP, β-actin, and control vector (pBSK^{+}) DNA are displayed in lanes 1–5 and 7–10. Lanes 6 and 11 show ethidium bromide (EtBr) staining of DNA probes. Veh., vehicle. (*B*) Schematic representation of NR DBS present in the mouse TSLP gene. The A base of the translation initiation codon (ATG) was taken as +1. Every indicated DBS recruited its cognate NRs in vivo in at least one of the examined tissues. (*C*) ChIP assays using WT mouse epidermis, treated as indicated, show the binding of RXR-α and VDR to TSLP DR3 DBS. Ab IP, antibodies used for immunoprecipitation. (*D*) ChIP assays using epidermis from WT and VDR$^{ep-/-}$ mice to reveal VDR and RXR-α recruitment to the TSLP DR3d region. (*E*) ChIP assays using epidermis from WT and RAR-γ$^{-/-}$ mice to probe RAR and RXR-α recruitment to the TSLP DR2b DBS. (*F*) ChIP assays using Veh. and RA-treated epidermis to reveal RAR and RXR binding to the indicated DBS. (*G*) Quantitative RT-PCR (Q-RT-PCR) of genes, as indicated, from epidermis of WT and RAR-γ$^{-/-}$ mice topically treated for 16 h. (*H*) ChIP assays using epidermis from WT and various keratinocyte-selective NR mutant (Mut) mice to detect VDR and RAR binding to indicated DBS. (*I*) ChIP assays using epidermis and ileal and colonic epithelium from WT mice to reveal RAR and RXR-α binding to different DR2 DBS, as indicated. (*J*) ChIP assays of WT mouse epidermis to reveal RXR-α binding to TSLP DR1 elements, as indicated. (*K*) Q-RT-PCR of TSLP and PPAR-γ RNA from ileal and colonic epithelium of WT and PPAR-γ$^{iec-/-}$ mice injected i.p. with rosiglitazone (Rosi.). (*L*) ChIP assays using ileum and colon epithelium isolated from WT mice injected i.p. with Veh. or Rosi. to detect PPAR-γ and RXR-α binding to indicated TSLP DR1 DBS. All Q-RT-PCR values are mean ± SEM.

Results

VDR, RARs, and RXRs Control TSLP Expression at the Transcriptional Level in Mouse Epidermal Keratinocytes. To investigate whether MC- and RA-induced increases in TSLP RNA level in epidermis of wild-type (WT) mice (2) are due to increased transcription, nuclear run-on assays were performed using epidermis of WT mice treated with vehicle (ethanol), MC, or RA. TSLP-specific run-on transcript signals were exclusively detected in MC- and RA-treated samples (Fig. 1*A*,

lanes 1–3). Moreover, run-on transcripts after MC treatment produced a stronger signal than the signal generated by RA, indicating that a higher TSLP RNA level achieved with MC versus RA (2) was due to a higher rate of transcription. Similarly, cotreatment with MC and RA generated a stronger TSLP signal (Fig. 1*A*, lane 4), in agreement with the synergistic increase observed at the RNA level (2). Epidermis from RXR-αβ$^{ep-/-}$, RAR-γ/VDR$^{ep-/-}$, and RAR-αγ/VDR$^{ep-/-}$ mice (Fig. 1*A*, lanes 8–10) was subjected to nuclear run-on assays, whereas β-actin transcription was measured to ensure that an equal amount of nuclei was used across the various samples and the pSK^{+} vector served as a negative control (Fig. 1*A*). In all cases, increases in TSLP RNA (Fig. 2 *B*–*E*) and in protein levels (Fig. 2 *F* and *G*) were correlated with increased transcription from the TSLP promoter (Fig. 1*A*).

Unliganded RXR-α/VDR and RXR-β/RAR-γ Heterodimers Bind to Their TSLP Cognate Response Elements, but Activation of Transcription Requires the Presence of Agonistic Ligands. We previously noted the presence of several putative NR DBS in the mouse TSLP gene upstream promoter region (2). Allowing for two base mismatches in NR consensus DBS, a thorough "ocular" and bioinformatics analysis of 100-kb upstream and 20-kb downstream DNA sequences from the mouse TSLP +1 position (considering "A" of the translation initiation codon ATG as position +1) revealed seven putative VDREs (DR3a–DR3g), two putative RAREs (DR2a–DR2b), and three putative DR1 DBS (DR1a–DR1c) known to bind RXRs heterodimerized with either peroxisome proliferator-activated receptor (PPAR), liver X receptor (LXR), or farnesoid X receptor (FXR), among others (Figs. 1*B* and 5*A* and Table S1). Note that DR3b, DR3c, and DR3e DBS, as well as DR3d, DR3f, and DR3g DBS, contain identical sequences (Table S1), whereas DR3f and DR3g DBS are present within a 2.13-kb-long repeated sequence spanning positions −32,824 to −30,694 (encompassing DR3f) and −44,655 to −42,526 (encompassing DR3g).

Binding of their cognate NRs to these DBS was analyzed in vitro by electrophoretic mobility shift assay (EMSA) and supershift assay, using epidermal nuclear extracts (NEs) and the respective antibodies. Only DR3d, DR3f, and DR3g formed a complex that was supershifted with RXR-α and VDR antibodies. Because DR3d, DR3f, and DR3g have identical sequences (Table S1), only DR3d

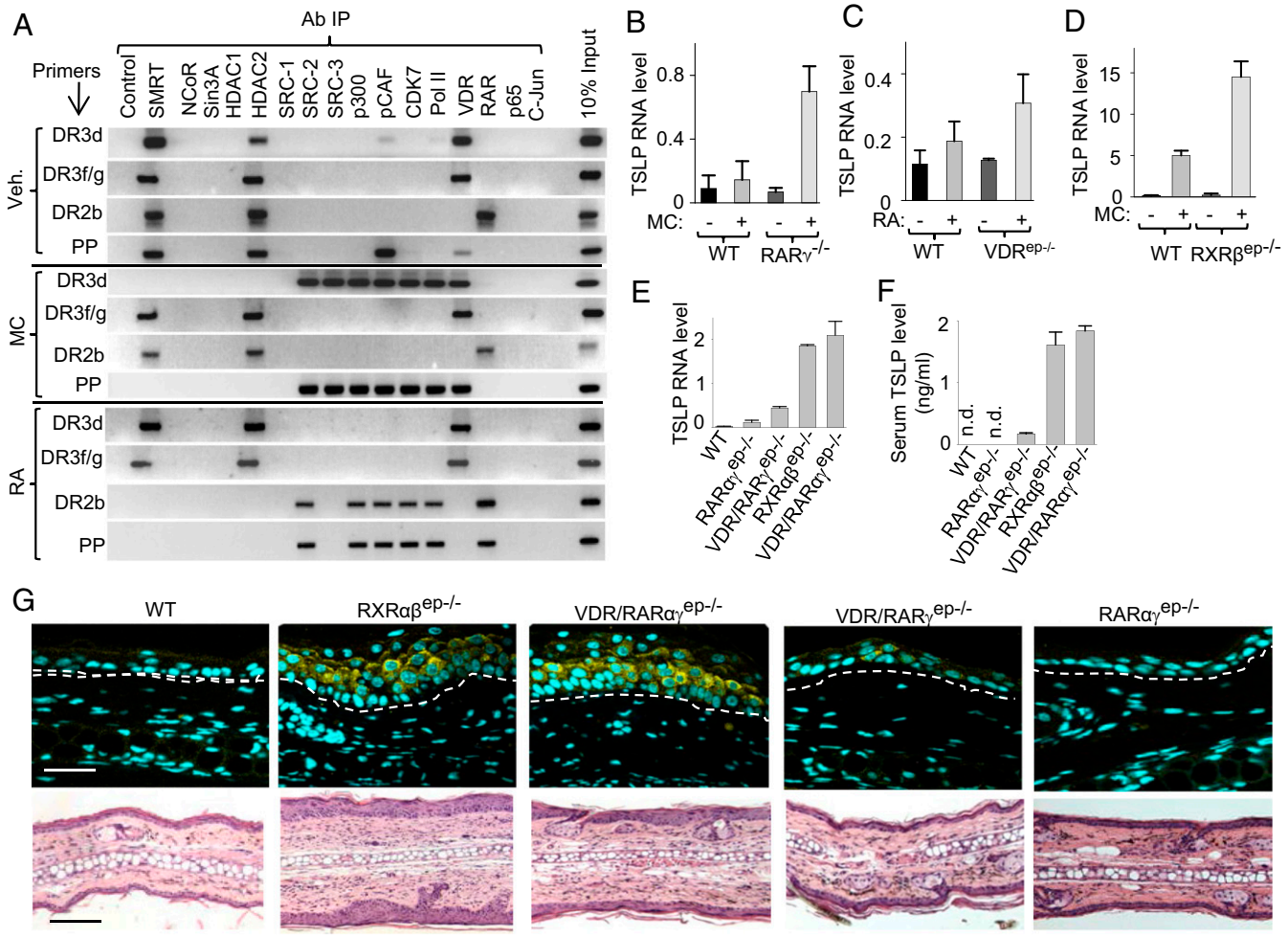

Fig. 2. Repressing and activating complexes are assembled by association of RXR-β/RAR-γ and RXR-α/VDR on TSLP DR2 and DR3 DBS, as well as on the PP region, in the absence and presence of their cognate ligands, respectively. (*A*) ChIP assays performed from WT mouse dorsal epidermis, treated as indicated. (*B*) TSLP Q-RT-PCR from WT and RAR-γ$^{-/-}$ mice treated with 0.25 nmol MC. (*C*) TSLP Q-RT-PCR from WT and VDR$^{ep-/-}$ mice treated with 1 nmol RA per ear. (*D*) TSLP Q-RT-PCR from WT and RXR-β$^{ep-/-}$ mice treated with 4 nmol MC per ear. (*E*) TSLP Q-RT-PCR from ears of WT and mutant mice, as indicated, 2 wk after the first Tam injection. (*F*) Serum TSLP level in the mice used in Fig. 2*E*. n.d., not detected. (*G*) TSLP immunohistochemistry (*Upper*) and hematoxylin/eosin (HE) staining (*Lower*) images of ear sections of WT and mutant mice, as indicated. The dotted line indicates the epidermis/dermis junction. (*Upper*) Yellow and cyan colors reveal the staining of TSLP and nuclei, respectively. Note the different degrees of epidermal hyperproliferation and dermal cell infiltration in HE-stained ear sections of mutant mice. (Scale bars: 25 μm, *Upper*; 100 μm, *Lower*.) In *B*–*D*, all Q-RT-PCR values are mean ± SEM. All topical treatments to the ear were performed for 16 h.

was tested. Importantly, this complex was absent in NE from VDR$^{ep-/-}$ mice (Fig. S1*A*). Both DR2a and DR2b complexes were shifted by RXR-α and RAR-γ antibodies (Fig. S1*B*), whereas only DR1a- and DR1b-bound complexes were supershifted by RXR-α, PPAR-α, and PPAR-γ antibodies (Fig. S1*C*; no efficient PPAR-β antibody was available for supershift). MC, RA, fenofibrate (PPAR-α agonist), or rosiglitazone (PPAR-γ agonist) treatment did not affect VDR, RAR, and PPAR binding to their response elements in vitro. None of these NR DBS were perfect consensus elements, and only those NR DBS containing at least one consensus repeated motif associated with the corresponding NR (Table S1).

We then tested whether DR3, DR2, and DR1 DBS were associated with their corresponding NR partners in epidermis. Using RXR-α and VDR antibodies, and irrespective of MC treatment, chromatin immunoprecipitation (ChIP) assays from vehicle-treated epidermis revealed the association of VDR and RXR-α with DR3d and DR3f/g DBS (Fig. 1*C*) but, as expected, not with DR3a and DR3b. Because DR3f and DR3g are present within a repeat sequence, unique primers could not be designed specifically to assess VDR and RXR-α binding to these regions. The specificity of the ChIP assay was confirmed by the lack of VDR and RXR-α binding to the DR3d DBS in epidermis of VDR$^{ep-/-}$ mice (Fig. 1*D*). A similar pattern was observed for VDR and RXR-α binding to the DR3d and DR3f/g DBS in WT mouse IEC (Fig. 5 *A*–*C* and Fig. S1*D*).

Because no "ChIP-grade" antibody specific against RAR isotypes was available, a pan-RAR antibody (reacting with all three RAR isotypes) was used to investigate whether a RAR could associate with TSLP DR2 DBS. Irrespective of RA treatment, neither a RAR nor RXR-α was associated with the DR2a DBS in epidermis, whereas under identical conditions, a RAR was bound to the DR2b DBS (Fig. 1*F*). To identify the RAR isotype associated with the TSLP DR2b DBS, we performed ChIP assays using epidermis from RAR-γ$^{-/-}$ mice. No binding of RAR with DR2b was detectable, indicating that RAR-γ selectively associated with DR2b (Fig. 1*E*). The specific involvement of the RAR-γ isotype in regulation of TSLP transcription was confirmed by using the isotype-specific RAR agonistic ligands BMS961 and BMS753 (8), which are selective for RAR-γ and RAR-α, respectively. Measurement of TSLP RNA level in WT and RAR-γ$^{-/-}$ mice treated with these ligands revealed that both RA and BMS961, but not BMS753, enhanced TSLP levels in WT animals, whereas none of these ligands increased TSLP levels in RAR-γ$^{-/-}$ mice (Fig. 1*G*). As a control, the above ligands were tested for the induction of CRABPII RNA [a known RA target gene (9)]. In WT mice, RA, BMS961, and BMS753 could increase CRABPII RNA level, but RA and BMS961 were more efficient than BMS753. As expected, in RAR-γ$^{-/-}$ mice, only RA and BMS753 could weakly induce CRABPII RNA (Fig. 1*G*).

Surprisingly, RXR-α could not be detected on the DR2b DBS (Fig. 1*F*). We therefore tested whether RXR-α/RAR heterodimers could associate with the DR2 DBS present in the CRABPII gene. Both RXR-α and RAR were detected on the CRABPII DR2 (Fig. 1*F*), indicating that the lack of RXR-α association with the DR2b DBS was specific to the TSLP gene. Whether RAR-γ could be selectively heterodimerized with RXR-β instead of RXR-α on the TSLP DR2b region was investigated using ChIP assays carried out with epidermis from RXR-α$^{ep-/-}$, RXR-β$^{ep-/-}$, and RXR-αβ$^{ep-/-}$ mice. As expected, VDR binding was unaffected in RXR-β$^{ep-/-}$ mice, whereas RAR-γ association decreased by ∼90% in these mice (Fig. 1*H*), thus indicating that VDR was heterodimerized with RXR-α, whereas RAR-γ was mostly associated with RXR-β. Accordingly, in RXR-α$^{ep-/-}$ mice, VDR did not associate with DR3d DBS (Fig. 1*H*), whereas RAR-γ binding to the DR2b DBS was decreased by ∼30% (Fig. 1*H*). As expected, neither VDR nor RAR-γ associated with its cognate DBS in RXR-αβ$^{ep-/-}$ mice. Interestingly, RAR bound to the CRABPII DR2 with equal efficiency in both WT and RXR-β$^{ep-/-}$ mice, whereas RAR binding was decreased by more than 80% in RXR-α$^{ep-/-}$ mice and no significant binding was detected in RXR-αβ$^{ep-/-}$ mice (Fig. 1*H*), thus indicating that RAR-γ was mostly heterodimerized with RXR-α on the CRABPII DR2 RARE.

In contrast to epidermis, ChIP with WT mouse IEC from ileum and colon revealed RAR-γ and RXR-α associations with the TSLP DR2a DBS, whereas neither RAR nor RXR-α was detected at the DR2b DBS (Figs. 1*I* and 5 *A*–*C*). The CRABP II DR2 DBS in IEC showed a similar NR binding pattern as in epidermis (Fig. 1*I*).

To identify NRs bound to the TSLP DR1 DBS (Fig. 5*A*), ChIP was performed using RXR-α, PPAR-α, and PPAR-γ antibodies. Only RXR-α binding to the DR1a DBS was detected in epidermis (Fig. 1*J*). Skin topical treatment with PPAR agonists (fenofibrate and rosiglitazone) could not induce TSLP expression. In contrast, rosiglitazone increased the TSLP RNA level in the IEC of WT mouse and IEC-selective ablation of PPAR-γ (PPAR-γ$^{iec-/-}$) abolished this increase (Fig. 1*K*). ChIP assays using colonic cells further demonstrated the constitutive association of PPAR-γ and RXR-α to the DR1b and DR1c DBS, and rosiglitazone induced the binding of PPAR-γ and RXR-α to the DR1a region (Fig. 1*L*). In contrast, in WT ileal IEC, constitutive binding of PPAR-γ and RXR-α occurred only on the DR1c region, whereas DR1a, DR1b, and DR1c all bound PPAR-γ and RXR-α upon rosiglitazone treatment (Figs. 1*L* and 5*C*). Irrespective of treatments with cognate agonists, PPAR-α and PPAR-β binding could not be detected with any of the TSLP DR1-DBS in IEC.

Taken together, these results demonstrated that (*i*) RXR-α selectively heterodimerizes with VDR on TSLP DR3 DBS; (*ii*) RXR-α is also the predominant partner of RAR on the CRABPII DR2 DBS; (*iii*) RXR-β is the predominant partner of RAR-γ on the TSLP DR2b DBS in epidermis; (*iv*) RXR-β may partially substitute for RXR-α binding on the CRABPII DR2 element in epidermis of RXR-α$^{ep-/-}$ mice; (*v*) RXR-α could be weakly redundant with RXR-β on the TSLP DR2b DBS; and (*vi*) there are striking differences in patterns of RAR/RXR-heterodimer binding to TSLP RAREs in IEC and epidermis, as well as differential rosiglitazone induction patterns of TSLP expression mediated by DR1 PPRE in IEC, thus illustrating the tissue-specific control of TSLP transcription by NRs (Fig. 5 *A*–*C*).

In the Absence and Presence of Their Cognate Ligands, VDR/RXR-α and RAR-γ/RXR-β Assemble Repressing and Activating Complexes, Respectively, on TSLP VDRE and RARE. Because unliganded RXR-α/VDR and RXR-β/RAR-γ heterodimers are "constitutively" bound to their DBS on the TSLP gene in the absence of any treatment of epidermis, we investigated whether these heterodimers could be functionally active in repressing TSLP transcription. It is known that in the absence of agonistic ligands, DNA-bound RXR/VDRs and RXR/RARs assemble repressing complexes containing corepressors and histone deacetylases (HDACs), thereby establishing a transcriptionally inactive state (10). ChIP with WT epidermis revealed the presence of SMRT and HDAC2, (but not HDAC1, HDAC3, and HDAC7) on DR3d, DR3f, and/or DR3g and DR2b DBS (Fig. 2*A*). On the other hand, following MC treatment, the corepressors SMRT and HDAC2 disappeared from DR3d DBS, and we observed the appearance of the SRC2 (TIF2) and SRC3 coactivators, as well as p300, pCAF, and CDK7 TFs and RNA polymerase II (Pol II). In contrast, the DR3f and/or DR3g DBS, as well as the DR2b DBS, were still associated with corepressors. On the other hand, RA treatment resulted in loss of SMRT and HDAC2 and recruitment of SRC2 (but not of SRC3), as well as p300, pCAF, CDK7, and Pol II specifically to the DR2b DBS (Fig. 2*A*). To assess the overall transcription status of the TSLP promoter, we amplified the proximal promoter region (−318 to −8 bp from position +1; hereafter, PP). In untreated epidermis, the PP region was associated with SMRT, HDAC2, and pCAF, as well as VDR to a much lesser extent. Treatment with MC or RA resulted in dissociation of SMRT and HDAC2 and in association of SRC2 and SRC3 (SRC3 was seen only in MC-treated samples), as well as p300, pCAF, CDK7, and Pol II, on the PP region (Fig. 2*A*). In the ileum

and colon, irrespective of VD3 treatment, the DR3d DBS was constitutively associated with SRC2, SRC3, and Pol II, along with RXR-α and VDR, whereas the DR3f/DR3g region recruited SMRT with RXR-α and VDR (Fig. S1 *D* and *E*).

Because both VDR/RXR-α and RAR-γ/RXR-β assembled repressing complexes in untreated epidermis, we aimed at identifying which of the two complexes was the dominant one. Ears of WT and RAR-$\gamma^{-/-}$ mice were treated with a limiting dose of MC (0.25 nmol per ear). No significant increase in TSLP RNA was observed in WT mice, whereas an approximately fivefold increase was observed in RAR-$\gamma^{-/-}$ mice (Fig. 2*B*). On the other hand, treatment of WT and VDR$^{ep-/-}$ mice with RA at a dose of 1 nmol per ear resulted in an ∼1.5-fold increase and a twofold increase in TSLP RNA level, respectively (Fig. 2*C*), suggesting that the RAR-γ–associated repressor complex played a dominant role in repressing TSLP transcription. In agreement with these results, treatment of RXR-β$^{ep-/-}$ mice with 4 nmol of MC per ear resulted in an ∼150-fold increase in TSLP RNA level, in comparison to only an ∼50-fold increase in WT mice (Fig. 2*D*).

We then investigated whether RAR-α was involved in the repression of TSLP expression. Because unliganded RXR-α/VDR and RXR-β/RAR-γ heterodimer complexes appeared to be responsible for the repression of TSLP transcription in WT mice epidermis, we assumed that selective ablation of VDR and RAR-γ in keratinocytes should result in increased TSLP expression, similar to the increased TSLP expression observed in RXR-αβ$^{ep-/-}$ mice. Therefore, we generated conditional knockout mice lacking both RAR-γ and VDR in keratinocytes (RAR-γ/VDR$^{ep-/-}$ mice). Although increases in TSLP RNA and protein levels were observed in these mice, they were lower than the levels observed in RXR-αβ$^{ep-/-}$ mice (Fig. 2 *E* and *F*, also Fig. 1*A*). Moreover, these mice did not develop the pathological phenotype typical of RXR-αβ$^{ep-/-}$ mice, as judged by the external ear phenotype (2) and histological analysis (epidermal hyperproliferation and dermal immune cell infiltrate; Fig. 2*G*). Interestingly, mice selectively lacking RAR-α in addition to RAR-γ and VDR in keratinocytes (RAR-αγ/VDR$^{ep-/-}$) developed a pathological phenotype closer to RXR-αβ$^{ep-/-}$ mice (Fig. 2*G*). As expected, the levels of TSLP RNA and protein in the RAR-αγ/VDR$^{ep-/-}$ triple mutants were comparable to the levels in RXR-αβ$^{ep-/-}$ mice (Fig. 2 *E* and *F*, also Fig. 1*A*). That RAR-γ/VDR$^{ep-/-}$ mutants exhibited a milder pathological phenotype than RXR-αβ$^{ep-/-}$ mutant mice may reflect a redundancy between RAR-α and RAR-γ isotypes such that when RAR-γ is ablated, RAR-α could substitute for some of its repressor activity. However, treatment of RAR-γ/VDR$^{ep-/-}$ mice with the RAR-α–selective BMS753 ligand did not result in any further increase in TSLP RNA, and we could not detect any RAR-α bound at the DR2b DBS in these mutants, which suggests the alternate possibility that ablation of RAR-αγ/VDR or RXR-αβ in the keratinocytes could activate additional TFs, which would, in turn, induce TSLP transcription.

Taken together, these ChIP assays and the nuclear run-on assays (within their limit of sensitivities) demonstrate that in WT epidermis, heterodimers of VDR/RXR-α and RAR-γ/RXR-β are bound to their respective DBS on the TSLP gene, along with the corepressors SMRT and HDAC2, thereby maintaining the TSLP gene in a transcriptionally inactive state. Upon MC or RA treatment, SMRT and HDAC2 are released from the DNA-bound NR complexes, followed by recruitment of SRC2- and/or SRC3-bearing coactivator complexes, leading to TSLP expression. Importantly, although all three DR3 DBS (DR3d, DR3f, and DR3g) could associate with RXR-α, VDR, SMRT, and HDAC2, only the DR3d DBS could recruit coactivators upon VD3 treatment (Fig. 2*A*), indicating that not all VDRE-bound RXR-α/VDR complexes are able to function as transcriptional activators even in the presence of an agonistic ligand. Interestingly, the constitutive assembly of an activating complex of VDR, RXR-α, SRC2, SRC3, and Pol II at the DR3d DBS in IEC suggested that VD3 could be instrumental in TSLP expression in these cells (11).

Multiple Functional Smad, STAT, NF-κB, and Activator Protein 1 DBS Are Present in the TSLP Promoter Region. A bioinformatics analysis across 100 kb upstream and 20 kb downstream from the TSLP +1 translation initiation codon revealed the presence of several putative Smad, NF-κB, activator protein 1 (AP1), and STAT DBS (Fig. 5*A*). The TSLP upstream promoter region contains two putative Smad DBS (Fig. 3*A* and Table S1). In EMSAs, both Smad a and Smad b DBS could bind Smad3 and Smad4 (Fig. S2*A*). ChIP assays with WT epidermis, as well as with mouse lung epithelial 12 (MLE12) cells, revealed that Smad2, Smad3, and Smad4 could bind to Smad a and Smad b DBS (Fig. S2*B*). Additionally, pCAF was constitutively bound to these regions. However, no Smad binding was detected at the PP region in mouse epidermis, whereas it was readily detected at the TSLP PP region in MLE12 cells (Fig. S2*B*). Smad binding to its cognate DBS and PP was further enhanced by TGF-β treatment of the MLE12 cells (Fig. S2*B*). Smad2 or Smad3 binding to Smad DBS was not detected in Smad2$^{ep-/-}$ or Smad3$^{ep-/-}$ mice, respectively, confirming the specificity of ChIP antibodies (Fig. S2*C*). The functionality of Smads in regulating TSLP transcription was investigated by treating MLE12 cells with TGF-β and either a Smad3-specific inhibitor (SIS3) (12) or a TGF-β receptor–specific inhibitor (TGFR In) (13). Treatment with either SIS3 or TGFR In repressed the basal level of TSLP transcript by 25%, whereas TGF-β treatment stimulated TSLP transcript level by ∼30%, which was prevented by the inhibitors (Fig. 3*B*). The specificity of these inhibitors was ensured by determining Smad7 expression [a TGF-β target (14)], which showed the expected decrease (Fig. 3*B*).

Seven consensus STAT6 DBS (STAT6a–STATg) and one consensus STAT5 DBS [STAT5a (15, 16)] are located in the TSLP gene (Fig. 5*A* and Table S1). Interestingly, ChIP assays revealed that STAT5 was bound in epidermis to STAT6 and STAT5a DBS only after 12-O-tetradecanoylphorbol-13-acetate (TPA) treatment of mouse skin (Fig. S2*D*), whereas no STAT6 binding was detectable at any of these DBS. Overnight MC treatment did not induce STAT5 or STAT6 binding; however, 3 d of MC treatment (once daily) resulted in STAT5 binding to several STAT DBS (Fig. S2*D*). Neither STAT5 nor STAT6 binding was detected after 3 d of RA treatment (Fig. S2*D*). These observations were further verified in MLE12 cells treated with VD3, IL-1β, or TPA, which revealed a constitutive association of STAT5 and STAT6 to STAT6a–STATd DBS (Fig. S2*E*). VD3 treatment did not alter this pattern. However, IL-1β treatment resulted in the disappearance of STAT5 and increased STAT6 binding to the same DBS (Fig. S2*E*). Taken together, these data indicate a redundancy among STAT6 DBS present on the TSLP gene for STAT5 and STAT6 binding, and also suggest a (likely) contribution of STAT5 and/or STAT6 in mediating TPA- and/or MC-induced TSLP transcription in mouse epidermis and MLE12 cells.

One consensus NF-κB and five imperfect NF-κB DBS are present in the mouse TSLP gene (Fig. 5*A* and Table S1). Lee and Ziegler (17) reported that the "upstream" NF-κBc DBS were instrumental in NF-κB–mediated expression of the mouse TSLP gene. In EMSA, using TPA-treated epidermal NE, we found that the mouse NF-κBa element bound the p65 and p50 NF-κB components much more efficiently than the NF-κBc element (Fig. S3*A*). The in vivo association of "NF-κBa and NF-κBc" DBS with the p65 subunit was tested by ChIP assays. In vehicle and MC- or RA-treated epidermis, p65 was not bound to any of the TSLP NF-κB DBS (Fig. 3*C*). This lack of binding was due to a lack of NF-κB activation; following TPA treatment, the p65 subunit was recruited to NF-κBa and NF-κBc DBS (Fig. 3*C*), with the binding to NF-κBa being much more efficient than the binding to NF-κBc (Fig. 3*C*). A functional role of NF-κB in activating TSLP expression in epidermis was revealed by cotreatment with TPA and (E)3-[(4-methylphenyl)-sulfonyl]-2-propenenitrile

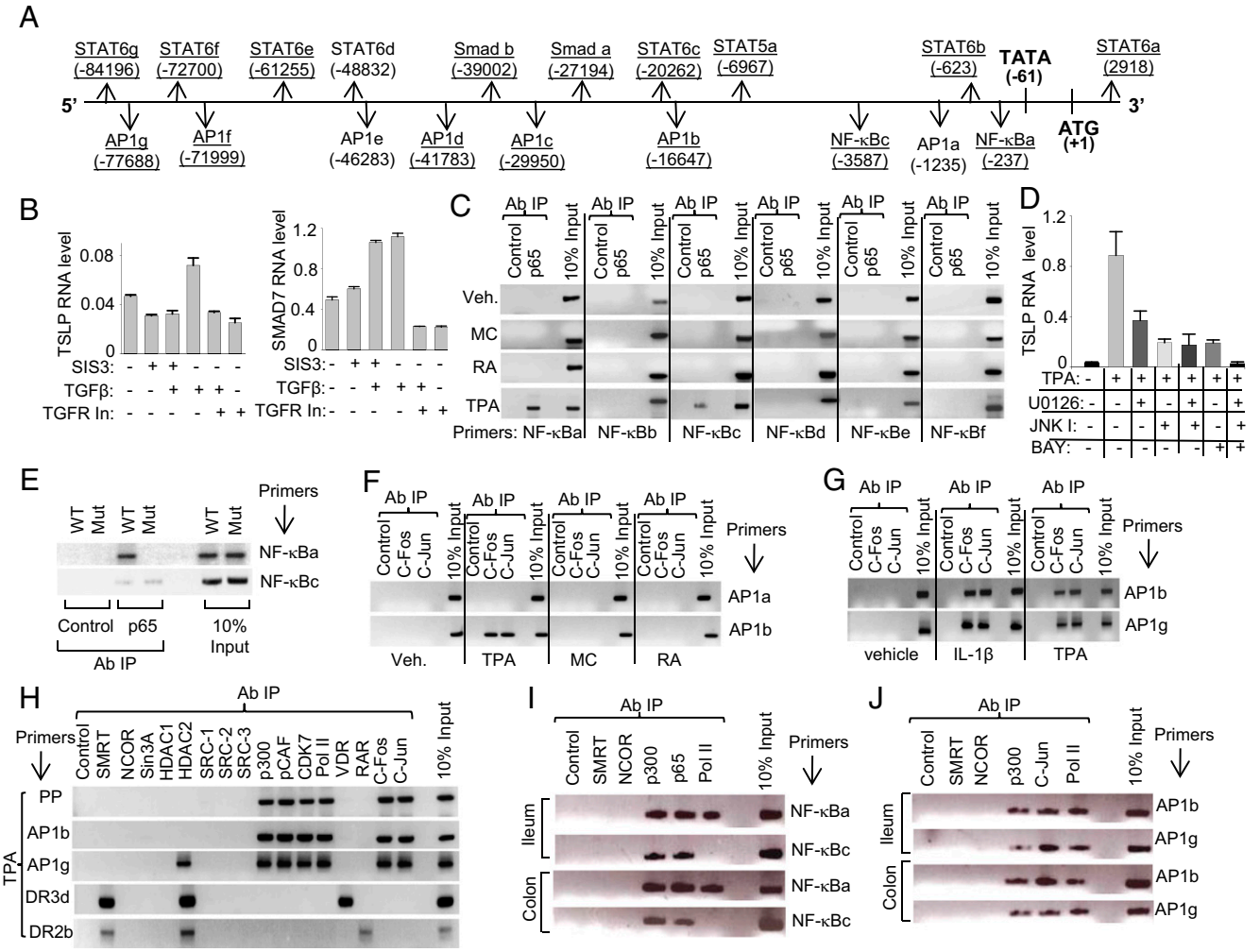

Fig. 3. TSLP transcription is controlled by multiple Smad, STAT, NF-κB, and AP1 DBS. (*A*) Schematic location of TF DBS present in the mouse TSLP gene. The underlined DBS bind their cognate TFs in ChIP assays using epidermis isolated from WT mice. (*B*) Q-RT-PCR of indicated transcripts from MLE12 cells treated for 6 h, as indicated. (*C*) ChIP assays using WT mouse epidermis, treated as indicated, to detect p65 binding to putative NF-κB DBS. (*D*) TSLP Q-RT-PCR from ears of WT mice treated for 6 h, as indicated. (*E*) ChIP assays using TPA-treated dorsal epidermis of WT and NF-κBa$^{-/-}$ (Mut) mice to detect p65 binding to TSLP NF-κBa and NF-κBc DBS. (*F*) ChIP assays using WT mouse dorsal epidermis, treated as indicated, to detect c-Fos and c-Jun binding to AP1a and AP1b DBS. (*G*) ChIP assays using IL-1β– or TPA-treated MLE12 cells to reveal c-Fos and c-Jun binding to TSLP AP1b and AP1g DBS. (*H*) ChIP assays from TPA-treated WT mouse dorsal epidermis using indicated antibodies. (*I*) ChIP assays from WT mouse ileal and colonic epithelium using antibodies, as indicated, for TSLP NF-κBa and NF-κBc DBS. (*J*) ChIP assays from WT mouse ileal and colonic epithelium using antibodies, as indicated, for TSLP AP1b and AP1g DBS. All Q-RT-PCR values are mean ± SEM.

(BAY 11-7082; BAY) (a specific inhibitor of IKK-β activity; 18), which resulted in an ∼70% decrease in TSLP RNA level (Fig. 3*D*), in keeping with nuclear run-on assays showing that topical TPA treatment enhances the rate of TSLP transcription (Fig. 1*A*, lane 5). To determine whether NF-κB stimulated the TSLP promoter when activated by a physiologically relevant inducer, MLE12 cells were treated with IL-1β or TPA. The level of TSLP RNA was indeed increased (Fig. S3*C*), whereas p65 and p50 proteins did bind to NF-κBa DBS, and bound much less efficiently to NF-κBc DBS (Fig. S3*D*). A null mouse mutant (NF-κBa$^{-/-}$ null, in which the NF-κBa DBS were deleted) was engineered to evaluate the function of these DBS in vivo. As expected, upon topical TPA treatment, no p65 binding was observed on the NF-κBa DBS of NF-κBa$^{-/-}$ null mice (Fig. 3*E*), whereas the weak binding on the NF-κBc DBS was unaffected. However, there was no significant decrease in TPA-induced TSLP RNA synthesis in NF-κBa$^{-/-}$ mice, most likely due to a concomitant TPA induction of AP1 activity (discussed below). Interestingly, Cultrone et al. (19) reported that the NF-κBa DBS are conserved in humans and play a crucial role in TSLP expression, whereas the NF-κBc DBS have a minor role. This preeminent role of the NF-κBa DBS has also been confirmed in the mouse by Negishi et al. (20), who also unveiled an interesting synergy in activation of TSLP expression by the IFN regulatory factor IRF3 and NF-κB via IRF DBS and NF-κB DBS located in close vicinity.

The mouse TSLP gene contains four consensus (b, e, f, and g) and three imperfect (a, c, and d) AP1 DBS (Fig. 3*A* and Table S1). In EMSA and supershift assays with TPA-treated epidermal NE, both the consensus and imperfect AP1 elements equally bound c-Fos and c-Jun (Fig. S3*B*). In ChIP assays using epidermis from vehicle, MC-treated mice, or RA-treated mice, c-Fos and c-Jun were not bound to any of the TSLP AP1 DBS (Fig. 3*F*). However, upon TPA treatment, which is known to induce AP1 activity (11), ChIP assays using epidermal extract revealed that both c-Fos and c-Jun could bind to AP1 (b–d, f, and g) DBS (Fig. S3*E*). As expected, cotreatment of skin with TPA and the extracellular regulated kinase inhibitor U0126 or the Jun kinase inhibitor resulted in an ∼50% and 70% decrease in the level of TSLP transcript, respectively (Fig. 3*D*). Similar association of c-Fos and c-Jun with the TSLP AP1 DBS was also revealed by ChIP assays using MLE12 cells treated with IL-1β or TPA to activate c-Fos and c-Jun (Fig. 3*G*).

ChIP assays were performed using TPA-treated epidermis to identify coactivators present at NF-κB and AP1 DBS. Owing to the close proximity of the NF-κBa DBS (−237 bp) with the PP region, PCR with PP primers was used to detect factors present at both the NF-κBa and PP regions. TPA treatment resulted in the binding of p300, CDK7, Pol II, p65, and c-Jun to the PP region (Fig. 3*H*), in addition to pCAF, which was also detected in the absence of TPA (Fig. 2*A*). None of these factors except p65 (discussed above) were detected at the NF-κBc DBS. AP1b and AP1g DBS were also associated with the same factors, except that, in addition, HDAC2 was present at AP1g (Fig. 3*H*). No cofactors were detected at the AP1c, AP1d, and AP1f DBS, although they recruited c-Fos and c-Jun (Fig. S3*E*). Note that both DR3d and DR2b DBS were associated with their respective NRs and corepressors in the presence of TPA (Fig. 3*H*), indicating that dissociation of corepressors from these DBS is not a prerequisite for transcriptional activation of the TSLP promoter by NF-κB and AP1.

Most notably, both NF-κBa and NF-κBc DBS, as well as AP1b and AP1g DBS, were found to be constitutively associated with p65, p50 (Fig. S3*F*), and c-Fos and c-Jun (Fig. S3*G*; also Fig. 5*C*), respectively, in the IEC of WT mouse. Moreover, NF-κBa-, AP1b-, and AP1g-containing regions were also constitutively associated with coactivator p300 and Pol II (Fig. 3 *I* and *J*), indicating that these regions are transcriptionally active.

Treatments with VD3, RA, and TPA Induce Chromatin Loops Between the Regions Containing Their Respective Response Elements and the PP Region of the TSLP Gene. Direct interactions between regions containing DBS for activating complexes and PP regions are known to be instrumental in initiation of transcription (21, 22). Because DR3d and PP; DR2b and PP (Fig. 2*A*); and AP1b, AP1g, and PP (Fig. 3*H*) regions displayed similar cofactor dynamics in the presence of their respective agonists, we hypothesized that the DR3d, DR2b, AP1b, and AP1g DBS located in the upstream regulatory region may be interacting through a chromatin loop with the PP region in an activation-dependent manner. A chromatin conformation capture (3C) assay was performed on epidermal chromatin of mice topically treated with various activating compounds to test this possibility. Chromatin was digested with the AluI enzyme to separate fragments encompassing regions of interest (Fig. 4*A*), which were then ligated to reveal possible interactions between them.

In the absence of MC, no interaction was observed between the DR3d and PP regions, whereas MC treatment resulted in a clear interaction between them in the WT mice, and, as expected, no interaction between the DR3d and PP regions was observed in VDR$^{ep-/-}$ mice treated with MC (Fig. 4*B*). Moreover, DR3f and/or DR3g, which did not show any coactivator or Pol II binding (Fig. 2*A*), failed to interact with the PP region (Fig. 4*B*). Similarly, 3C assays using a DR2b region-specific probe revealed a selective interaction between the DR2b and PP regions in the presence of RA (Fig. 4*C*). Interestingly, 3C assays performed to determine the interaction between different AP1 element-containing regions with the PP region revealed that only the AP1b and AP1g elements were associated with the PP region upon TPA treatment (Fig. 4*D*).

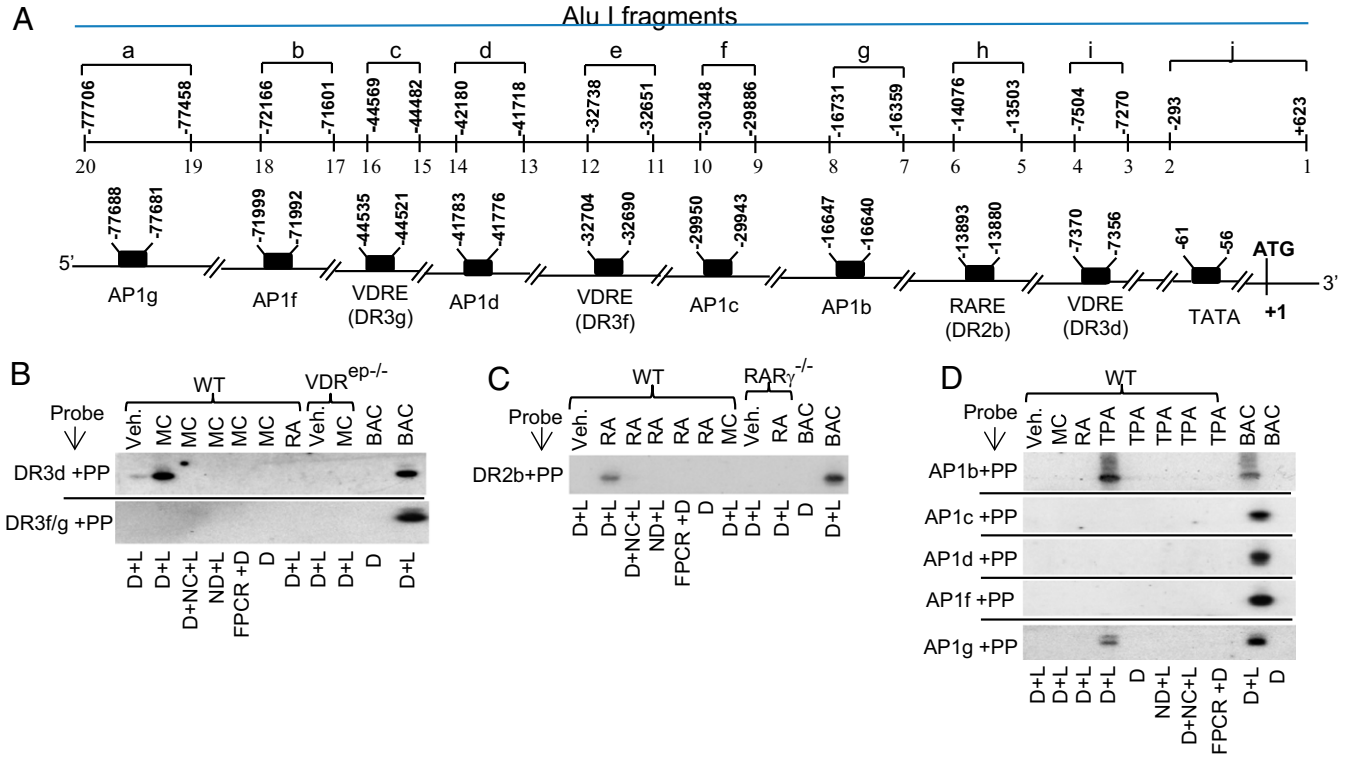

Fig. 4. MC, RA, or TPA treatment induces an interaction between the different regions that contain the respective cognate factor DBS (VDR, RARs, or AP1) and the PP region of the TSLP gene. (*A*) Mouse TSLP promoter and upstream region. The A base of the translation initiation codon (ATG) is represented by +1, and a–j are AluI-digested DNA fragments. The numbers 1–20 denote AluI sites. Boxes represent DBS for the indicated TFs with their coordinates. (*B*) Using skin epidermis from WT and VDR$^{ep-/-}$ mice treated as indicated, the 3C assays reveal the interaction between the regions containing DR3d and PP and DR3f/DR3g and PP. (*C*) Using dorsal skin epidermis of WT and RAR-γ$^{-/-}$ mice, treated as indicated, the 3C assays reveal the interaction between the DR2b and PP regions. (*D*) Using WT mouse dorsal epidermis, treated as indicated, the 3C assays detect a possible interaction between regions that contain different AP1 DBS and the PP regions, as indicated. D, Alu I digested; FPCR + D, final PCR product digested with AluI before Southern blotting; L, ligated; NC, not cross-linked; ND, not digested.

Discussion

Several NRs Differentially Control the Expression of TSLP in Epidermal Keratinocytes and IEC. TSLP is an important immune-regulatory cytokine that is expressed in several cell types, including the epithelial cells at barrier surfaces, such as the skin, lung, and intestine. It acts on cells of both myeloid and lymphoid lineages to promote T helper 2 (Th2) differentiation and Th2 cytokine-associated inflammation (23, 24). Constitutive TSLP expression in IEC confers tolerance against commensals (25). IEC-expressed TSLP also plays a critical role in mediating the recovery from colonic inflammation (26). In contrast, exacerbated expression of TSLP in keratinocytes, the lungs, and the esophagus correlates with the onset of various allergic diseases, such as AD, asthma, and food allergy-associated eosinophilic esophagitis (6, 27, 28). Collectively, these data illustrate various physiological and pathophysiological roles of TSLP throughout life, thus suggesting that strict spatiotemporal control of TSLP expression is essential for maintaining homeostasis. Our previous studies (1–3), as well as the studies of other groups (17, 29), have generated preliminary evidence regarding the mechanisms that control TSLP expression. In the present study, we have performed a detailed analysis of the *cis*-acting regulatory elements that control TSLP transcription in vivo in mouse epidermal keratinocytes and IEC. Our results unequivocally establish the role of the NRs VDR and RAR-γ in controlling TSLP transcription in keratinocytes of mouse epidermis. Unliganded heterodimers of RXR-α and VDR, together with unliganded heterodimers of RXR-β and RAR-γ, associated with the corepressors SMRT and HDAC2 are constitutively associated with their cognate DBS located in the TSLP upstream regulatory region (Fig. 2*A*). This mode of active repression by two different NR-associated repressor complexes ensures a tight control over TSLP expression, which is crucial for maintaining skin homeostasis.

Most interestingly, our study also reveals that the function of the multiple RXR and RAR isotypes is not redundant in vivo when bound as heterodimers to either a given DBS in different genes in a given tissue or the same DBS in different tissues (Fig. 5 *B* and *C*). In epidermal keratinocytes, and irrespective of the presence of their cognate ligands, VDR is heterodimerized with RXR-α on the DR3d, DR3f, and DR3g VDREs of the TSLP promoter, whereas RAR-γ is heterodimerized with RXR-β on the DR2b RARE of the TSLP gene and heterodimerized with RXR-α on the DR2b RARE of the CRABP II gene (Figs. 1 *F* and *H* and 2*A*). Derepression of TSLP expression via keratinocyte-selective ablation of either RXR-α and RXR-β (RXR-αβ$^{ep-/-}$ mutants) or RAR-γ(α) and VDR (RAR-γ/VDR$^{ep-/-}$ or RAR-γα/VDR$^{ep-/-}$ mutants) results in the release of repressor complexes from their respective DBS and recruitment of the transcriptional machinery, thus initiating TSLP transcription (Fig. 1*A*). The role of RAR-α remains elusive, because we did not detect its binding to the DR2b DBS or an increase in TSLP transcript level upon application of a RAR-α–specific agonist (Fig. 1*G*).

Analysis of IEC revealed that the binding pattern of VDR and RXR-α on the DR3 VDREs is the same as in epidermis (Fig. S1*D*). However, in contrast to epidermis, no RAR-γ/RXR-α heterodimers are bound to the DR2b RARE; instead, they are bound to the DR2a RARE (Figs. 1*I* and 5 *B* and *C*). Along the same lines, although no PPAR isotypes in epidermis were found to be associated with any of the TSLP DR1 DBS, PPAR-γ was associated with all three DR1 DBS in IEC, where TSLP transcription was induced by rosiglitazone (Figs. 1 *J*–*L* and 5 *B* and *C*). These data demonstrate the complexity of TSLP transcriptional regulatory mechanisms and illustrate in vivo tissue-specific variations of the binding of a particular NR-isotype to cognate DBS. It would be of interest to explore through which epigenetic mechanism the accessibility of RAR-γ/RXR-α to the DR2a and DR2b sites, as well as the accessibility of RXR-α/PPAR-γ to DR1 DBS, is differentially controlled in epidermis and IEC.

Even though unliganded VDR/RXR-α–associated repressor complexes could be detected on all three DR3d, DR3f, and/or DR3g DBS, only DR3d recruited a coactivator complex upon MC treatment (Fig. 2*A*), which raises important questions regarding the physiological role of these DR3 DBS. Does only DR3d modulate TSLP transcription and do DR3f/g-bound VDRs behave only as repressors, or do they recruit coactivators under particular instances? It remains to be investigated whether epigenetic mechanisms (e.g., histone modifications, DNA methylations) prevent the recruitment of coactivators to the DR3f/g DBS. Note that the DR3f/g region also does not appear to interact with the PP region in the presence of MC (Fig. 4*B*), whereas fragments encompassing the DR3d and PP regions interact with each other (Fig. 4*B*), and, furthermore, identical sets of coactivators and Pol II are detected on both the DR3d and PP regions in VD3-treated samples (Fig. 2*A*), therefore suggesting the formation of an "activating" loop between the DR3d and PP regions (Fig. 4*B*). Note that, in IEC, where VD3 is synthesized (30), the DR3d DBS are constitutively functional (Fig. S1*E*). Similarly, topical treatment of mouse epidermis with RA induced the transcription of TSLP, which was accompanied by the formation of a loop resulting from interaction between the chromatin fragment encompassing the DR2b DBS and PP regions, and by the presence of an identical set of coactivators and Pol II at both regions (Figs. 2*A* and 4*C*). Interestingly, we have shown that both loops are destroyed upon binding of the liganded glucocorticoid (GC) receptor (GR) to the TSLP inverted repeat negative GR element (IRnGRE) (11). Finally, it is puzzling that even though both VD3 and RA induce TSLP synthesis in the epidermal suprabasal layers (2), only the SRC2 coactivator was recruited to the DR2b and PP regions upon RA treatment, whereas both SRC2 and SRC3 coactivators were recruited to the DR3d and PP regions in VD3-treated epidermis (Fig. 2*A*).

NF-κB, AP-1, STAT, and Smad Transactivators Are also Differentially Involved in the Control of TSLP Expression. We have characterized multiple NF-κB, AP1, STAT, and Smad DBS in the sequences upstream and downstream of the mouse TSLP start site. We detected "constitutive" binding of Smads (Smad2–Smad4) to the Smad DBS in the TSLP gene in WT mice and in MLE12 cells (Fig. S2 *B* and *C*). However, their functional relevance in regulating TSLP transcription in vivo remains unclear. We have also shown that STAT5 and STAT6 are differentially recruited to STAT DBS depending on the stimulus (Fig. S2 *D* and *E*). Interestingly, it has been shown that TSLP induces STAT5 activity in cultured cells (31). Could TSLP be involved in regulating STAT5 activity at the TSLP promoter? Identification of multiple functional STAT DBS in the TSLP promoter region may point to the prevalence of a positive feedback loop that drives TSLP transcription in a STAT-dependent manner.

We have shown that ablation of the NF-κBa element within the TSLP promoter prevented the binding of the NF-κB p65 and p50 proteins. However, the actual contribution of this binding to the TPA-induced TSLP transcription could not be assessed because the NF-κBc and AP1 DBS remained "active" in the NF-κBa mutant. Analysis of the various AP1 DBS demonstrated that even though all of them are consensus DBS, only five of them (AP1b, AP1c, AP1d, AP1f, and AP1g) did associate with c-Fos and c-Jun in a TPA-dependent manner (Fig. S3*E*), and of these five, only the AP1b and AP1g DBS could be "functional" upon TPA treatment in epidermis through the formation of a chromatin loop with the PP region (Fig. 4*D*), thereby suggesting that only these two DBS are functional in epidermis. Interestingly, we have shown that in IEC, the microbiota-elicited Toll-like receptor signaling is the major determinant of both the NF-κB and AP-1 activity, and also that a reduction of this signaling leads to a decrease in TSLP expression in IEC (30). Additionally, microbiota-derived signaling is known to regulate RA synthesis in the

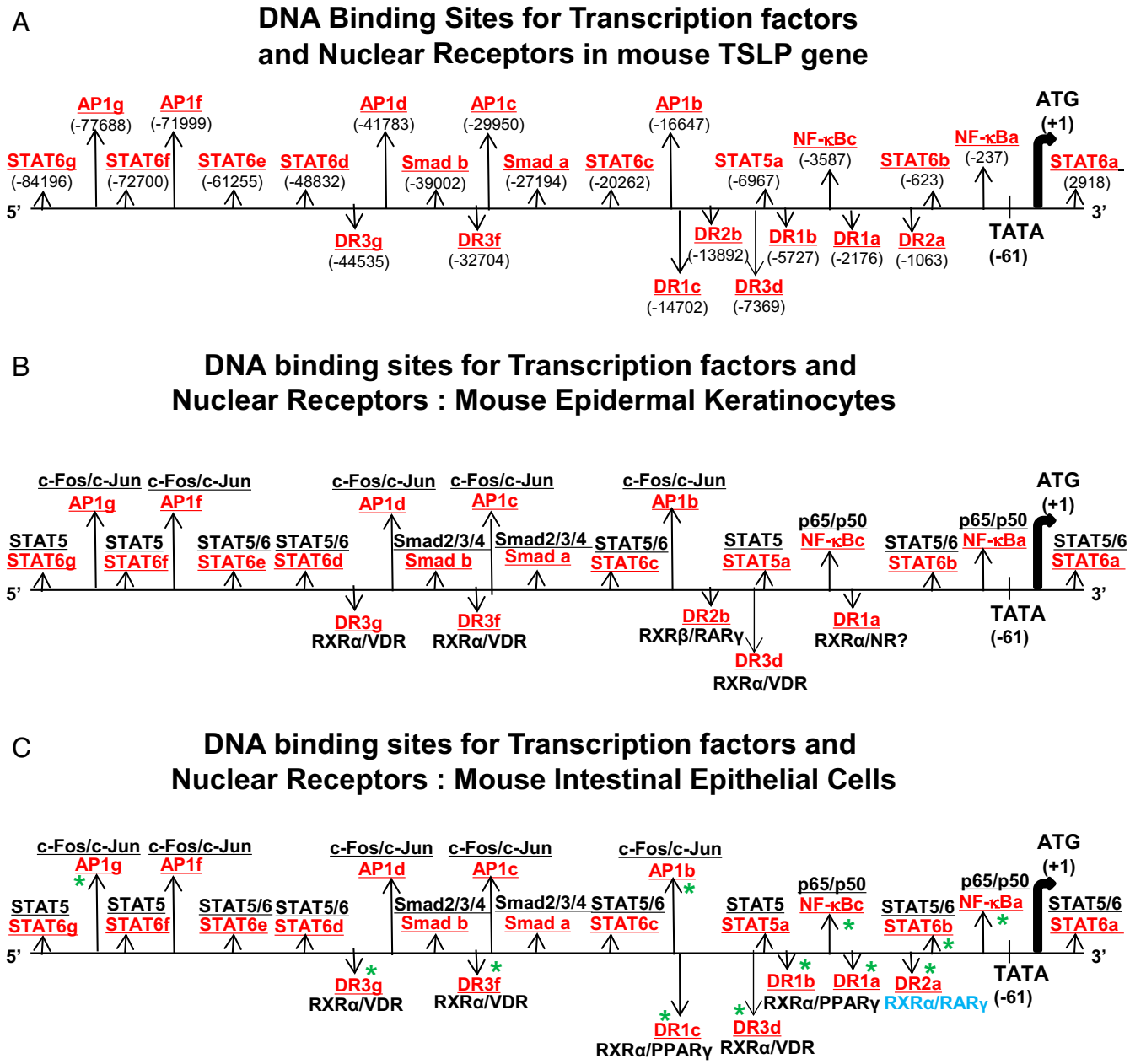

Fig. 5. Schematic representation of the mouse TSLP promoter-enhancer region. (*A*) In vivo DNA binding sites (DBS; indicated in red) for TFs and NRs located in the proximal and distal regions in the mouse TSLP gene. The A base of the translation initiation codon (ATG) was taken as +1 (also Table S1). (*B*) In epidermal keratinocytes of untreated WT mice, none of the TFs (except Smad2, Smad3, and Smad4) are recruited to their cognate DBS. Topical skin treatment with TPA or IL-1β to cells in culture induces NF-κB (p65/p50), AP1 (c-Fos/c-Jun), and STAT (STAT5/STAT6) binding, as well as TSLP transcription. Note that the indicated NR DBS are permanently occupied in vivo by their cognate NRs. All of the DBS are indicated in red. (*C*) In IEC of WT mice, the indicated (*) sites are permanently occupied. Note that in IEC, the DR2a DBS is functional and recruits RAR-γ/RXR-α heterodimer (indicated in blue), whereas the DR2b DBS is used in epidermis, in which RAR-γ/RXR-β is recruited. All of the DBS are indicated in red.

intestine (32), and we have recently found that a reduction in the microbiota signaling also reduces the expression of 25-(OH)D3 1-α-hydrodxylase (Cyp27B1, the rate-limiting enzyme in VD3 synthesis pathway) in IEC, thereby decreasing TSLP expression [by "inactivating" the DR3d DBS (30)]. Altogether, it appears that microbe-derived signaling in the "gut" is the major determinant of TSLP expression.

Taken together with other recent reports (11, 17, 20, 30), our present study provides an overall topological and functional map of the TSLP gene *cis*-acting regulatory elements, which are targeted by numerous signaling pathways to fine-tune the spatio-temporal regulation of TSLP expression, which is differentially exerted in two important epithelial tissues throughout life.

Methods

Mice. WT C57BL/6J mice, 6–8 wk old, were purchased from Charles River Laboratories. RXR-$\alpha^{ep-/-}$, RXR-$\beta^{ep-/-}$, RXR-$\alpha\beta^{ep-/-}$, RAR-$\gamma^{-/-}$, and VDR$^{ep-/-}$ are described (1, 2). RAR-γ/VDR$^{ep-/-}$ and RAR-αγ/VDR$^{ep-/-}$ were obtained by i.p. injection of tamoxifen (Tam) at a dose of 0.1 mg·d^{-1}, whereas PPAR-$\gamma^{iec-/-}$ was obtained by i.p. injection of Tam (1 mg·d^{-1}). For each case, Tam was injected for consecutive 5 d. Floxed smad2 and smad3 mice have been described (33). These mice were crossed with the K14 CreER^{T2} line to obtain floxed K14 CreER^{T2} smad2 and floxed K14 cre ER^{T2} smad3 animals. Smad2$^{ep-/-}$

and Smad3$^{ep-/-}$ mice were obtained by i.p. injection of Tam (1 mg·d^{-1}) for 5 d to the respective floxed animals. Age- and sex-matched littermates were used as WT controls. Breeding, maintenance, and experimental manipulations were approved by the Animal Care and Use Committee of the Institut de Génétique et de Biologie Moléculaire et Cellulaire/Institut Clinique de la Souris (ICS).

ChIP, Nuclear Run-On, and 3C Assays. ChIP assays were performed using chromatin prepared from 1% formaldehyde cross-linked keratinocytes and IEC, using indicated antibodies. Regions of interest were PCR-amplified using specific primers. Nuclear run-on was performed from nuclei isolated from epidermis, which were incubated in run-on buffer containing α-[^{32}P] UTP; following the transcription reaction, the nascent RNA was extracted and hybridized with DNA probes. The 3C assays were performed from formaldehyde cross-linked NE in epidermis, which was digested with AluI, and subsequently ligated and PCR-amplified to reveal the possible interactions. Detailed procedures, all primers, and probes are listed in *SI Materials and Methods*.

Quantitative RT-PCR, Serum TSLP Determination, Hematoxylin/Eosin Staining, and TSLP Immunohistochemistry. Quantitative RT-PCR was performed from the total RNA isolated from epidermis or IEC. Following isolation, RNA was reverse-transcribed to generate cDNA, which was used to detect indicated molecules. Paraformaldehyde-fixed ears were sectioned and stained with hematoxylin/eosin to reveal histopathological abnormalities. These sections were also immunoprobed with a specific antibody to detect TSLP protein in epidermis. Details are provided in *SI Materials and Methods*.

ACKNOWLEDGMENTS. We thank the staff of animal housing facilities at Institut de Génétique et de Biologie Moléculaire et Cellulaire/ICS for excellent help. We thank Martin Matzuk (Baylor College of Medicine) for floxed SMAD2 and SMAD3 mice. This work was supported by grants from the Association pour la Recherche a l'IGBMC (ARI) and the University of Strasbourg Institute for Advanced Study (USIAS). K.P.G., A.M., and M.S. were supported by fellowships from ARI and USIAS.

1. Li M, et al. (2005) Retinoid X receptor ablation in adult mouse keratinocytes generates an atopic dermatitis triggered by thymic stromal lymphopoietin. *Proc Natl Acad Sci USA* 102(41):14795–14800.
2. Li M, et al. (2006) Topical vitamin D3 and low-calcemic analogs induce thymic stromal lymphopoietin in mouse keratinocytes and trigger an atopic dermatitis. *Proc Natl Acad Sci USA* 103(31):11736–11741.
3. Li M, et al. (2009) Induction of thymic stromal lymphopoietin expression in keratinocytes is necessary for generating an atopic dermatitis upon application of the active vitamin D3 analogue MC903 on mouse skin. *J Invest Dermatol* 129(2):498–502.
4. Yoo J, et al. (2005) Spontaneous atopic dermatitis in mice expressing an inducible thymic stromal lymphopoietin transgene specifically in the skin. *J Exp Med* 202(4):541–549.
5. Angelova-Fischer I, et al. (2010) Injury to the stratum corneum induces in vivo expression of human thymic stromal lymphopoietin in the epidermis. *J Invest Dermatol* 130(10):2505–2507.
6. Soumelis V, et al. (2002) Human epithelial cells trigger dendritic cell mediated allergic inflammation by producing TSLP. *Nat Immunol* 3(7):673–680.
7. Liu YJ (2006) Thymic stromal lymphopoietin: Master switch for allergic inflammation. *J Exp Med* 203(2):269–273.
8. Chen JY, et al. (1996) Two distinct actions of retinoid-receptor ligands. *Nature* 382(6594):819–822.
9. Durand B, Saunders M, Leroy P, Leid M, Chambon P (1992) All-trans and 9-cis retinoic acid induction of CRABPII transcription is mediated by RAR-RXR heterodimers bound to DR1 and DR2 repeated motifs. *Cell* 71(1):73–85.
10. Glass CK, Rosenfeld MG (2000) The coregulator exchange in transcriptional functions of nuclear receptors. *Genes Dev* 14(2):121–141.
11. Surjit M, et al. (2011) Widespread negative response elements mediate direct repression by agonist-liganded glucocorticoid receptor. *Cell* 145(2):224–241.
12. Jinnin M, Ihn H, Tamaki K (2006) Characterization of SIS3, a novel specific inhibitor of Smad3, and its effect on transforming growth factor-beta1-induced extracellular matrix expression. *Mol Pharmacol* 69(2):597–607.
13. Gellibert F, et al. (2004) Identification of 1,5-naphthyridine derivatives as a novel series of potent and selective TGF-beta type I receptor inhibitors. *J Med Chem* 47(18):4494–4506.
14. Nakao A, et al. (1997) Identification of Smad7, a TGFbeta-inducible antagonist of TGF-β signalling. *Nature* 389(6651):631–635.
15. Ehret GB, et al. (2001) DNA binding specificity of different STAT proteins. Comparison of in vitro specificity with natural target sites. *J Biol Chem* 276(9):6675–6688.
16. Boucheron C, et al. (1998) A single amino acid in the DNA binding regions of STAT5A and STAT5B confers distinct DNA binding specificities. *J Biol Chem* 273(51):33936–33941.
17. Lee HC, Ziegler SF (2007) Inducible expression of the proallergic cytokine thymic stromal lymphopoietin in airway epithelial cells is controlled by NFkappaB. *Proc Natl Acad Sci USA* 104(3):914–919.
18. Kundu JK, Shin YK, Kim SH, Surh YJ (2006) Resveratrol inhibits phorbol ester-induced expression of COX-2 and activation of NF-kappaB in mouse skin by blocking IkappaB kinase activity. *Carcinogenesis* 27(7):1465–1474.
19. Cultrone A, et al. (2013) The NF-κB binding site located in the proximal region of the TSLP promoter is critical for TSLP modulation in human intestinal epithelial cells. *Eur J Immunol* 43(4):1053–1062.
20. Negishi H, et al. (2012) Essential contribution of IRF3 to intestinal homeostasis and microbiota-mediated Tslp gene induction. *Proc Natl Acad Sci USA* 109(51):21016–21021.
21. Liu Z, Garrard WT (2005) Long-range interactions between three transcriptional enhancers, active Vkappa gene promoters, and a 3′ boundary sequence spanning 46 kilobases. *Mol Cell Biol* 25(8):3220–3231.
22. Spilianakis CG, Flavell RA (2004) Long-range intrachromosomal interactions in the T helper type 2 cytokine locus. *Nat Immunol* 5(10):1017–1027.
23. Ziegler SF, Artis D (2010) Sensing the outside world: TSLP regulates barrier immunity. *Nat Immunol* 11(4):289–293.
24. Siracusa MC, et al. (2011) TSLP promotes interleukin-3-independent basophil haematopoiesis and type 2 inflammation. *Nature* 477(7363):229–233.
25. Rimoldi M, et al. (2005) Intestinal immune homeostasis is regulated by the crosstalk between epithelial cells and dendritic cells. *Nat Immunol* 6(5):507–514.
26. Reardon C, et al. (2011) Thymic stromal lymphopoetin-induced expression of the endogenous inhibitory enzyme SLPI mediates recovery from colonic inflammation. *Immunity* 35(2):223–235.
27. Rothenberg ME, et al. (2010) Common variants at 5q22 associate with pediatric eosinophilic esophagitis. *Nat Genet* 42(4):289–291.
28. Sherrill JD, et al. (2010) Variants of thymic stromal lymphopoietin and its receptor associate with eosinophilic esophagitis. *J Allergy Clin Immunol* 126(1):160–5.e3.
29. Mihály J, et al. (2016) TSLP expression in the skin is mediated via RARγ-RXR pathways. *Immunobiology* 221(2):161–165.
30. Mukherji A, Kobiita A, Ye T, Chambon P (2013) Homeostasis in intestinal epithelium is orchestrated by the circadian clock and microbiota cues transduced by TLRs. *Cell* 153(4):812–827.
31. Isaksen DE, et al. (1999) Requirement for stat5 in thymic stromal lymphopoietin-mediated signal transduction. *J Immunol* 163(11):5971–5977.
32. Hall JA, Grainger JR, Spencer SP, Belkaid Y (2011) The role of retinoic acid in tolerance and immunity. *Immunity* 35(1):13–22.
33. Li Q, et al. (2008) Redundant roles of SMAD2 and SMAD3 in ovarian granulosa cells in vivo. *Mol Cell Biol* 28(23):7001–7011.